

Electrochemical and Theoretical Examination of Some Imine Compounds as Corrosion Inhibitors for Carbon Steel in Oil Wells Formation Water

Arafat Toghan^{1,2*}, Ahmed Fawzy^{3,4}, Abbas I. Alakhras¹, Ahmed A. Farag^{5*}

¹Chemistry Department, College of Science, Imam Mohammad Ibn Saud Islamic University (IMSIU), Riyadh 11623, Saudi Arabia.

²Chemistry Department, Faculty of Science, South Valley University, Qena 83523, Egypt.

³Chemistry Department, Faculty of Applied Sciences, Umm Al-Qura University, Makkah 21955, Saudi Arabia.

⁴Chemistry Department, Faculty of Science, Assiut University, Assiut 71516, Egypt.

⁵Egyptian Petroleum Research Institute (EPRI), 11727 Cairo, Egypt

*E-mails: (A. Toghan) arafat.toghan@yahoo.com & aatahmed@imamu.edu.sa; (A.A. Farag) ahmedafm@yahoo.com

Received: 5 November 2022 / Accepted: 4 December 2022 / Published: 27 December 2022

The imine compounds (Z)-N-(2-(1-methyl-1H-pyrrol-2-yl)ethyl)-1-(thiophen-2-yl)ethan-1-imine (PSI) and (Z)-N-(2-(1-methyl-1H-pyrrol-2-yl)ethyl)-1-(pyridin-2-yl)ethan-1-imine (PPI) were effectively synthesized and described as corrosion inhibitors. The inhibition efficacy of PSI and PPI at carbon steel (CS) in formation water media was assessed using potentiodynamic polarization (PDP), electrochemical impedance spectroscopy (EIS) techniques, and quantum chemical calculations. PSI and PPI's inhibitory efficiency is related to the test's concentration. The maximum inhibitory efficiency was found in the presence of 1×10^{-3} M PSI and PPI, with 83 and 90 %, respectively. The two compounds are good mixed-type corrosion inhibitors, according to potentiodynamic polarization experiments. Both inhibitors' adsorption on CS surfaces followed the Langmuir adsorption isotherm, with both physisorption and chemisorption. Additionally, DFT studies and molecular dynamic (MD) simulation were used to explore the impact of PSI and PPI molecular on inhibition performance in formation water.

Keywords: Electrochemistry, Adsorption, Carbon steel, Imine compounds, Quantum chemistry calculation

1. INTRODUCTION

Carbon steel (CS) is utilized in a wide range of manufacturing, including chemical units, petroleum and gas manufacture, and construction constituents, because of their good mechanical

strength, good conduction, inexpensiveness, and ease of assemblage [1–3]. Corrosion poses a great threat to the safety of exploitation, transportation and storage of oil and gas formation water. Corrosion is a common form of problem in the oil and gas industries, which is one of the main considerations in the application of carbon and low alloy steels [4,5]. Hence, it is very imperative to effectively alleviate the corrosion of steels in formation water environments [6–9]. There have been numerous systems and strategies developed to protect metallic materials from oil and gas corrosion. Organic inhibitors confirmed as generally effective technology ways for preventing metal corrosion in adverse settings [10–12]. Organic corrosion inhibitors are usually made up of compounds having high electronic cloud with π -electrons of dual bonds, heteroatom donors like O, N, S, and P in their chemical composition [13,14]. As a result of the formed of protective layer at the metal substrate to guard averse to corrosive environment their physical and chemical adherent bulks on the steel have improved [15–17]. Schiff bases are useful chemicals used in drug, photochromic applications, and corrosion inhibitor [18,19]. Imine compounds, principally those utilized in the corrosion manufacturing, hinder corrosion in a variability of metals and its alloys, such as carbon steel, copper, and aluminum [20]. Schiff bases are highly popular more other organic materials as anticorrosive inhibitors because their availability, easy synthesis pathway, good purity, little toxicity, and environmentally friend [21]. Xiao-Long Li et al [22] investigated imine compounds related to aromatic pyridinyl compounds as a novel corrosion inhibitor for carbon steel in corrosive media. They claimed that the Schiff base's exitance 800 ppm reached 94% efficiency at 30 °C. In corrosive solution, Abdelmalik et al. [23] also looked at novel Schiff bases based on imidazole pyridine. They hypothesized that the efficiency of the inhibition increases with increasing inhibitor concentration and that these inhibitors simply decrease the cathode area without altering the cathodic reaction mechanism.

In this study, we used potentiodynamic polarization (PDP), and electrochemical impedance spectroscopy (EIS) to determine the corrosion inhibition efficacy of PSI and PPI in formation water. DFT has evolved into an influential technique to studying in what way molecule prearrangement in planetary and molecular assets effect inhibitor corrosion reserve effectiveness. Quantum chemical calculations are widely acknowledged as being significant in founding the relationship among molecules composition, chemical reactivity, and inhibitory selectivity [24]. DFT was utilized to comprehensively investigate the frontier orbitals of the inhibitor molecule's regular optimization assembly and electron mass spreading, as well as how quantum chemical variables influence the inhibitor's capacity to control corrosion. Therefore, the PSI and PPI reaction sites have been found to be sensitive to electron donation and receipt at the local level. PSI and PPI adsorption on the CS surface was also modelled using molecular dynamic (MD) simulations.

2. MATERIALS AND METHODS

2.1. Materials

For all synthesis purposes, analytical mark compounds and solvents have been utilized with no further purification. Sigma-Aldrich provided all of the necessary chemicals, including 2-(1-methyl-1H-pyrrol-2-yl)ethan-1-amine, 1-(thiophen-2-yl)ethan-1-one, and 1-(pyridin-2-yl)ethan-1-one. Al-Nasr Co.,

Egypt supplied methanol, ethanol, acetone, and oil formation water obtained from Qarun Petroleum Company, Egypt. The oil wells formation water with the chemical composition of: NaCl (65 ppm), KCl (5 ppm), CaCl₂ (1 ppm), NaHCO₃ (0.6).

2.2. Synthesis of PSI and PPI

Schiff bases (Z)-N-(2-(1-methyl-1H-pyrrol-2-yl)ethyl)-1-(thiophen-2-yl)ethan-1-imine (PSI) and (Z)-N-(2-(1-methyl-1H-pyrrol-2-yl)ethyl)-1-(pyridin-2-yl)ethan-1-imine (PPI) were obtained by addition of a solution of 2-(1-methyl-1H-pyrrol-2-yl)ethan-1-amine 0.01 mol in 10 mL methanol to a solution of 1-(thiophen-2-yl)ethan-1-one 0.01 mol in 10 mL methanol, or 1-(pyridin-2-yl)ethan-1-one 0.02 mol in 10 mL methanol and the reaction mixture refluxed for 1 h [25]. The product of precipitates of PSI and PPI were successively recrystallized by washing many times by C₂H₅OH, (CH₃)₂CO, and finally dried (Fig. 1). ¹H NMR of PSI (400 MHz, d₆-DMSO, 25 °C) δ_{ppm}: 1.8 (3H, N=C-**CH**₃), 2.6 (2H, methyl pyrrole-**CH**₂), 3.5 (3H, **CH**₃ attached to pyrrole group), 5.5 and 5.9 (2H, 2**CH** of pyrrole group), 7.3 (H, **CH** of pyrrole group beside N-CH₃), 8.2–8.3 (2H, 2**CH** of thiophene group). ¹H NMR of PPI (400 MHz, d₆-DMSO, 25 °C) δ_{ppm}: 1.8 (3H, N=C-**CH**₃), 2.6 (2H, methyl pyrrole-**CH**₂), 3.6 (3H, **CH**₃ attached to pyrrole group), 5.7 and 5.9 (2H, 2**CH** of pyrrole group), 7.1 (H, **CH** of pyrrole group beside N-CH₃), 8.1–8.6 (4H, 4**CH** of pyridine ring) (Fig. 2).

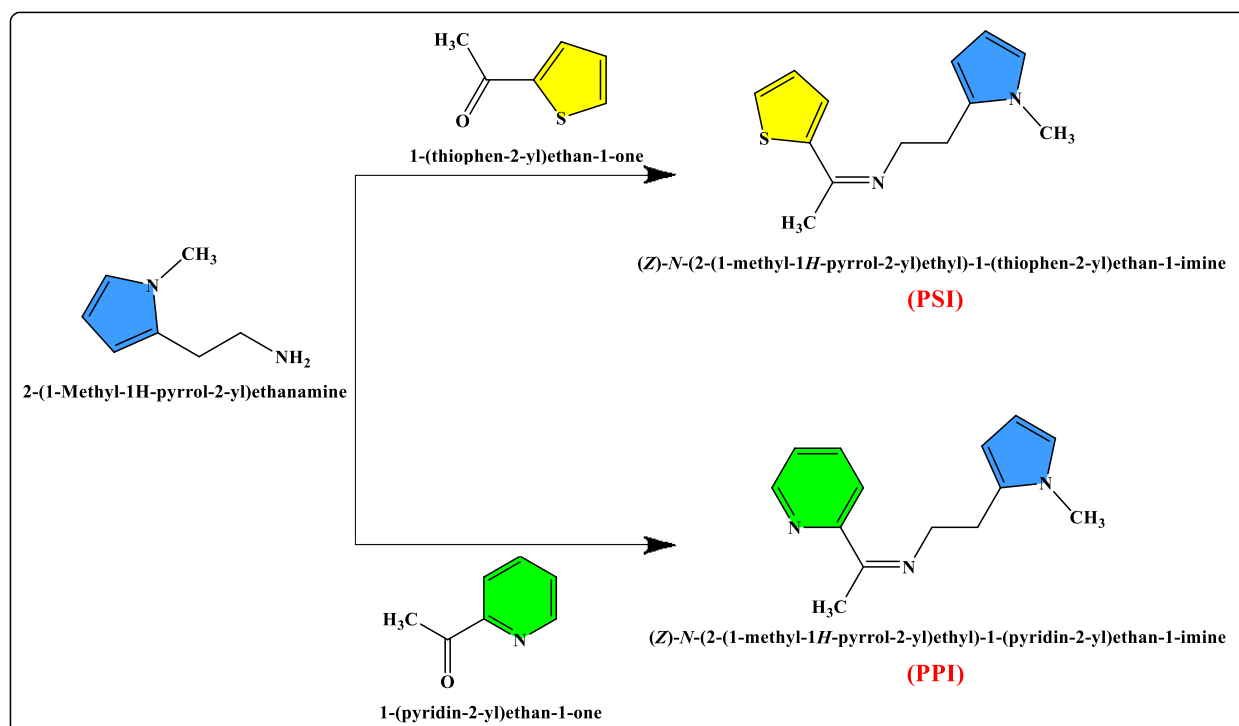


Figure 1. Preparation scheme of PSI and PPI.

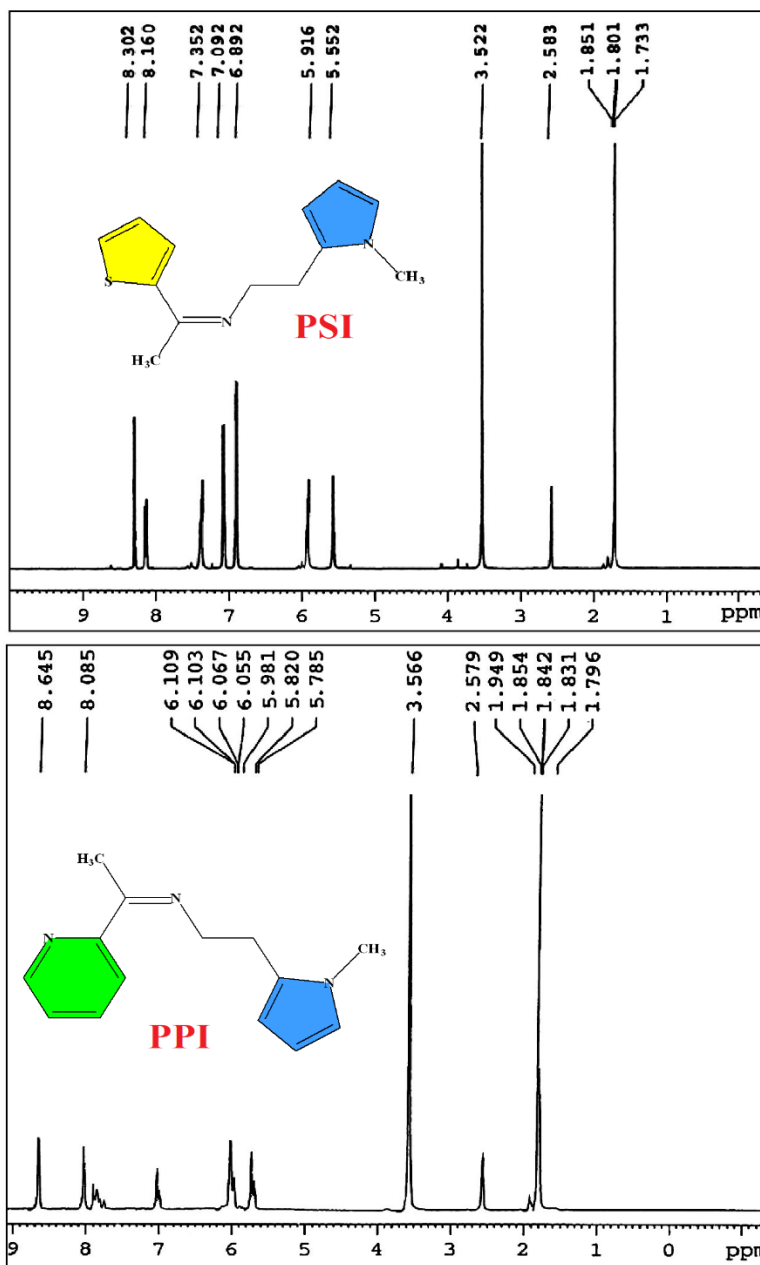


Figure 2. ¹H NMR charts of PSI and PPI inhibitors.

2.3. Specimens

With elemental iron making up the majority, carbon steel (CS) is made up of 0.21% carbon, 0.44% silicon, 0.39% manganese, 0.01% phosphorus, and 0.01% sulfur. On rod-shaped CS with a cross-exposed area of 0.5 cm², electrochemical impedance spectroscopy (EIS) and potentiodynamic polarization measurements were made. Each CS sample's surface was polished using emery sheets with a grade ranging from 400 to 2000. Following a thorough ultrasonic cleaning, the samples were degreased using the proper solvent, then dried.

2.4. Polarization and impedance experiments

The potentiodynamic polarization (PDP) and electrochemical impedance spectroscopy (EIS) studies were carried out using a three-electrode system. For the electrochemical cell, reference (saturated-calomel-electrode, SCE), auxiliary (Pt-electrode), and working electrodes (WE, CS-electrode) were utilized. Before the measurements, the WE were immersed in an electrochemical cell containing formation water or an inhibited solution for 1800 seconds to achieve a steady-state. The EIS is then performed with a frequency range of 0.01 Hz to 100 kHz and an amplitude of 5 mV. The PDP was performed in ± 0.25 V range at a scan rate of 0.5 mV s^{-1} .

2.5. DFT calculation details

Data on the regular optimization assembly and electron mass spreading of the inhibitor molecules were obtained using the Gaussian-9 software. Theoretical computations were performed at B3LYP and 6-311G (d,p) using atomic orbitals as the basis set and density functional theory (DFT) [26,27]. The energy of the Frontier (E_{HOMO} and E_{LUMO}) and the gap energy ($\Delta E = E_{\text{LUMO}} - E_{\text{HOMO}}$) were obtained through theoretical calculations to further define the inhibitions property.

2.6. Simulation studies

For the MD simulations, Material Studio 2017 software (Accelrys Inc.) was used, which were largely built on the Forcite module. Inhibitor molecules were tested in a simulated box with periodic border settings, ensuring that an illustrative area for restricted substrate was free of random border impact. Iron atom (110) was split lengthwise in a 5 sheet [28] and expanded into a (ten \times ten) supercell to validate a big enough surface for molecular communication [29].

3. RESULTS AND DISCUSSION

3.1. Potentiodynamic polarization (PDP) details

Potentiodynamic polarization measurements were carried out to assess the inhibitive effects of PSI and PPI. In the inhibitor-free and inhibitor-containing solutions, the potentiodynamic polarization of CS samples is depicted in Fig. 3. After adding inhibitors, it can be shown that the corrosion potential (E_{corr}) variation values toward anodic and cathodic directions are less than 85 mV, indicating that these inhibitors are mixed-type inhibitors for CS corrosion [30–32]. Table 1 contains a list of the potentiodynamic polarization's parameters, including E_{corr} , corrosion current density (i_{corr}), and the anodic and cathodic Tafel slopes (β_a , β_c). The following equation [33-35] can be used to compute the inhibition efficiency (η_{PDP} , %) of PSI and PPI:

$$\eta_i = \frac{i_{\text{corr}}^o - i_{\text{corr}}^i}{i_{\text{corr}}^o} \times 100 \quad (1)$$

where, respectively, i_{corr}^o and i_{corr}^i stand for the corrosion current densities in the uncontrolled and inhibited solutions. As the concentration of PSI and PPI rises, Table 1 shows that the i_{corr} steadily decreases. The presence of multiple adsorption sites on the CS surface for these chemicals, including the pyrrole group attached to the electron-donor methyl group, the imine group linked to another methyl group, the thiophene group in compound PSI, and the pyridine group in compound PPI, is what contributes to their higher η_{PDP} values. The results of η_{PDP} revealed that PPI rather than PSI can more successfully protect CS from corrosion caused by aggressive solutions, this is due to variances in their chemical structures. Due to the pyridine group's stronger conjugation system than the thiophene group's, PPI has a greater electronic cloud than PSI. The PPI inhibitor offers higher protection than PSI because it is more thoroughly adsorbed on the CS surface.

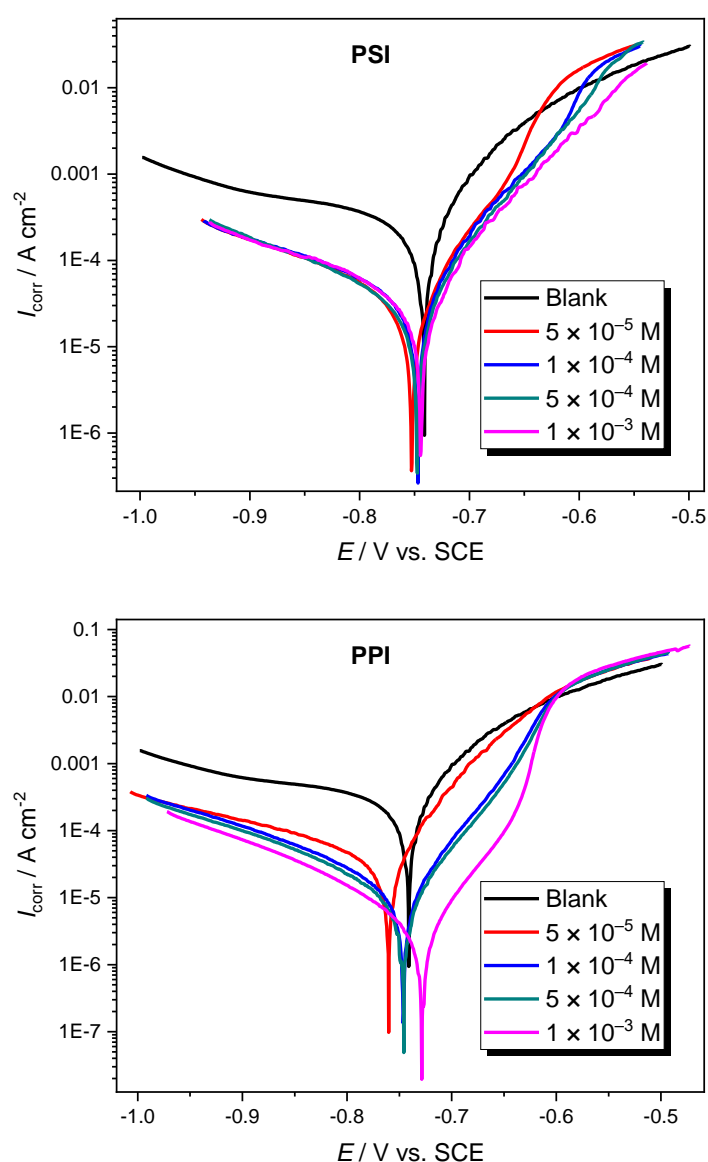


Figure 3. Potentiodynamic polarization curves for CS in oil wells formation water, unprotected and protected with different concentrations of PSI and PPI inhibitors.

Table 1. Polarization parameters of CS in oil wells formation water without and with various concentrations of inhibitors at 298 K

Inhibitors	C (M)	$-E_{\text{corr}}$ (mV)	i_{corr} (mA cm ⁻²)	β_a (mV dec ⁻¹)	$-\beta_c$ (mV dec ⁻¹)	θ	η_{PDP} (%)
Blank	Blank	739	0.2784	120	215	–	–
PSI	5×10^{-5}	750	0.1146	71	188	0.588	58.8
	1×10^{-4}	749	0.0907	65	181	0.674	67.4
	5×10^{-4}	751	0.0634	74	174	0.772	77.2
	1×10^{-3}	746	0.0475	77	183	0.829	82.9
PPI	5×10^{-5}	758	0.0881	64	192	0.684	68.4
	1×10^{-4}	742	0.0592	62	169	0.787	78.7
	5×10^{-4}	745	0.0371	65	158	0.867	86.7
	1×10^{-3}	733	0.0295	68	151	0.894	89.4

3.2. Electrochemical impedance spectroscopy (EIS) details

The characteristics of the interface assembly developed for metal surfaces can be precisely obtained through EIS experiments [36]. Resistance and capacitance, which are typically used to examine the progression of corrosion, are produced by the obtained EIS data. Therefore, it can be utilized regularly in the field of metal guard. CS corrosion Nyquist curves in formation water without and with PSI and PPI at various concentrations are shown in Fig. 4. All Nyquist curves can be seen to have a single loop, which indicates that charge transfer is primarily responsible for controlling the corrosion process [37]. With increasing PSI and PPI concentrations, the capacitive circle's width increased and was moulded into the CS substrate to resemble a corrosion fence film. Additionally, over the whole frequency range, the shapes of the Nyquist curves do not change when PSI and PPI concentrations increase. This shows that the implanted inhibitor molecules form a thin adsorption layer without altering the corrosion mechanism's properties [38]. This study indicated that the controller impact of PSI and PPI was coupled by their concentration in the layer that was produced [39]. Resistance quality indicates capacitance quality and corrosion defense ability, which repeat the value of the inhibitor molecule layer. Lower capacitance and higher resistance suggest the establishment of a dense and important protective layer [40]. The analogous chemical circuit shown in Fig. 5 was used with the ZSimpWin programme, which hysterically varies the impedance data, to estimate and modulate the impedance profile at the CS/media interface with different concentrations. Model (R(QR)) circuit is the most pertinent data in relation to the system under investigation. The resistance of the solution (R_s), the resistance of the charge transfer (R_{ct}), and the constant phase element (CPE) that should be present in the impedance profile are all used in this model circuit. The following equation [41] can be used to compute the percentage of inhibition (η_z):

$$\eta_z = \frac{R_{ct}^i - R_{ct}^o}{R_{ct}^i} \times 100 \quad (2)$$

where, respectively, R_{ct}^o and R_{ct}^i represent the charge transfer resistance of the CS in the formation water solution without and with an inhibitor.

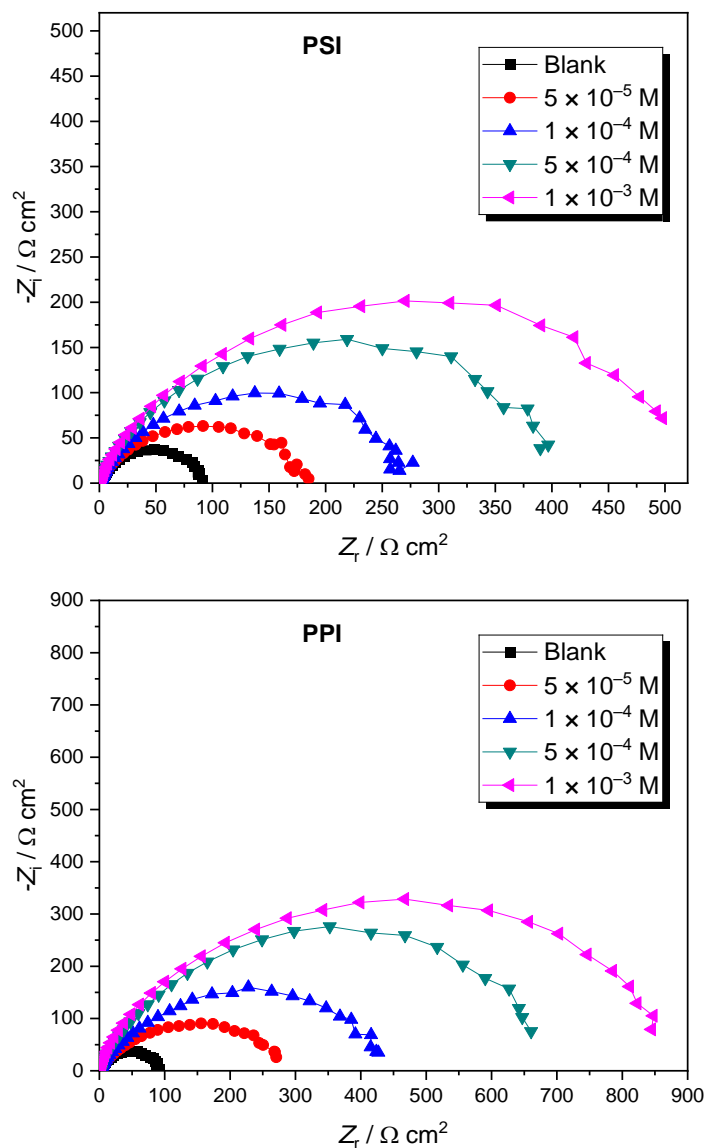


Figure 4. Nyquist plots for CS in oil wells formation water, unprotected and protected with different PSI and PPI inhibitors concentrations.

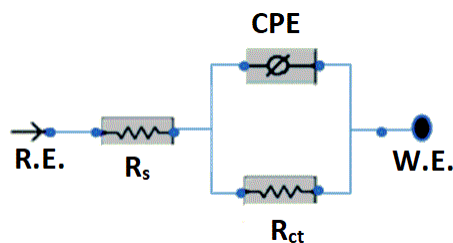


Figure 5. The equivalent circuit was used to fit the Nyquist plots.

The semicircle technique was used to estimate the EIS parameters exported for CS interaction with the corrosive formation water environment (Table 2). The constant phase element (CPE), which

may be created using the equation shown below [42–44], was created to reduce mistakes brought on by nonideal capacitance.

$$Z_{CPE} = \frac{1}{Q(j\omega)^n} \tag{3}$$

Where Q is the CPE degree proportionality factor, j is the number of unreal ($j^2 = -1$), ω is the frequency of angular ($\omega = 2\pi f$), and n stands for phase shift, which is related to surface morphology ($-1 \leq n \leq +1$). From Table 2, it can be seen that the value of R_{ct} rises when the PSI and PPI molecules are added, indicating that they adsorb at the CS surface and impede charge transfer, making the corrosion process even more difficult. Additionally, at a PSI and PPI concentration of 1×10^{-3} M, the highest percentages of inhibition, accounted for by 83.3% and 89.8%, respectively, were observed. The order of PPI > PSI was followed, and this result is in accordance with the potentiodynamic polarization.

Table 2. EIS parameters of MS in oil wells formation water without and with various concentrations of inhibitors at 298 K

Inhibitor	C (M)	R_s (Ω cm ²)	CPE		R_{ct} (Ω cm ²)	θ	η_z (%)
			Q ($\Omega^{-1}s^n$ cm ⁻²) $\times 10^{-5}$	n			
Blank	Blank	2.0	8.7	0.9	89	–	–
PSI	5×10^{-5}	1.6	5.8	0.8	185	0.519	51.9
	1×10^{-4}	1.4	9.5	0.8	275	0.676	67.6
	5×10^{-4}	1.4	7.7	0.9	415	0.786	78.6
	1×10^{-3}	1.5	6.9	0.8	533	0.833	83.3
PPI	5×10^{-5}	2.1	5.2×10^{-5}	0.9	294	0.697	69.7
	1×10^{-4}	1.8	4.1	0.8	441	0.798	79.8
	5×10^{-4}	1.7	2.1	0.9	690	0.871	87.1
	1×10^{-3}	2.2	9.3	0.9	875	0.898	89.8

3.3. Adsorption isotherm details

The ability of an inhibitor molecule to attach to a metal substrate in a corrosive environment must be evaluated [45]. The metal surface covering (θ) typically indicates the inhibitory activity. Based on the provided PDP and EIS data, the Langmuir isotherm can offer a good match with adsorption performance [46]. The lined regression factor of the Langmuir isotherm was found to be very close to unity. The Langmuir isotherm can be defined by the equation given below, Eq. [47]:

$$\frac{C}{\theta} = \frac{1}{K_{ads}} + C \tag{4}$$

where C represents for PSI and PPI concentration and K_{ads} stands for constant adsorption equipoise. The relationship between C/θ and C is obviously a straight line, with regression factors (R^2) for the slopes that are virtually equal and close to unity, as shown in Fig. 6 for both PSI and PPI inhibitor drugs.

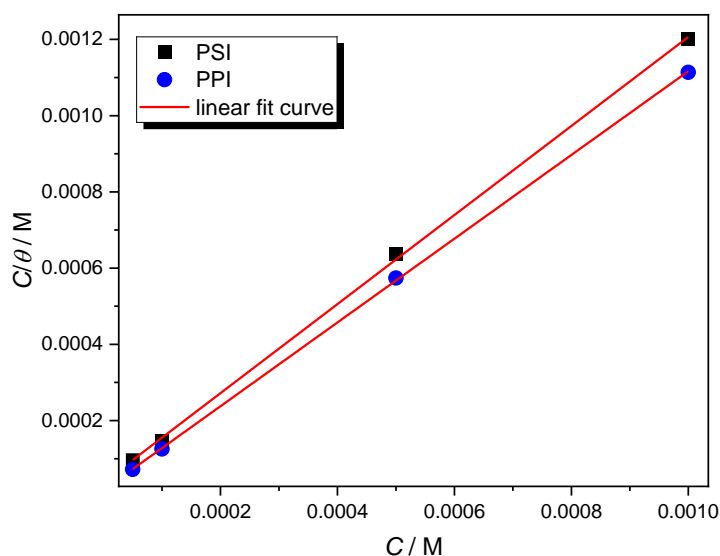


Figure 6. Langmuir adsorption isotherm for CS in oil wells formation water with different PSI and PPI inhibitor concentrations.

These results conclusively show that the PSI and PPI molecules stuck to the Langmuir model when they were absorbed onto the CS substrate [48-50]. By calculating the constant of adsorptive equipoise (K_{ads}) from the intercepts of the C/θ and C curves, which replicates the contact adsorption strength of PSI and PPI to the CS surface, the standard Gibbs' free energy (ΔG_{ads}) of adsorption may be derived using the following equation [51, 52]:

$$K_{ads} = \frac{1}{55.5} \exp\left(-\frac{(\Delta G_{ads})}{RT}\right) \quad (5)$$

The number 55.5 has to do with the molarity of the aqueous medium, factor R stands for the universal gas constant, and factor T stands for Kelvin temperature. As can be seen from Fig. 6, PPI has a higher K_{ads} value than PSI, which supports the fact that PPI has a stronger affinity for the CS substrate than PSI molecules. The minus values of the standard Gibbs' free energy clearly show that PSI and PPI spontaneously adsorb on the CS substrate. It can be determined that the adsorption of an organic molecule at a solid surface is of the physisorption type, which includes electrostatic contact among the organic molecules at a metal substrate, since it is generally agreed that the values of standard Gibbs' free energy are less than -20 kJ mol^{-1} . The adsorption of an organic molecule on a solid surface, however, could be classified as chemisorption type if the standard Gibbs' free energy values are greater than -40 kJ mol^{-1} [53]. This type of adsorption includes electronic distribution between the lone pair of organic molecules with the vacant d -orbital at the metal substrate. Our work's standard Gibbs' free energy data show that PSI and PPI with 35 and 37 kJ mol^{-1} adsorbed at the surface of CS via a mixed-type mechanism [54–61].

3.4. DFT calculations

The Gaussian-9 programme is used to modify the structure of PSI and PPI molecules, which is helpful for further uncovering the electrical properties of the particle and their active sites that assist the process of CS corrosion reserve. Fig. 7 reveals the optimum building of PSI and PPI. The molecules could be divided into lowest unoccupied molecular orbital (LUMO) and highest occupied molecular orbital (HOMO) according to frontier molecular orbital theory (LUMO). Due to their nature, HOMO and LUMO play a crucial role in the process of inhibiting corrosion. The LUMO portion of a molecule measures its ability to accept electrons, whereas the HOMO portion measures its ability to release electrons [62].

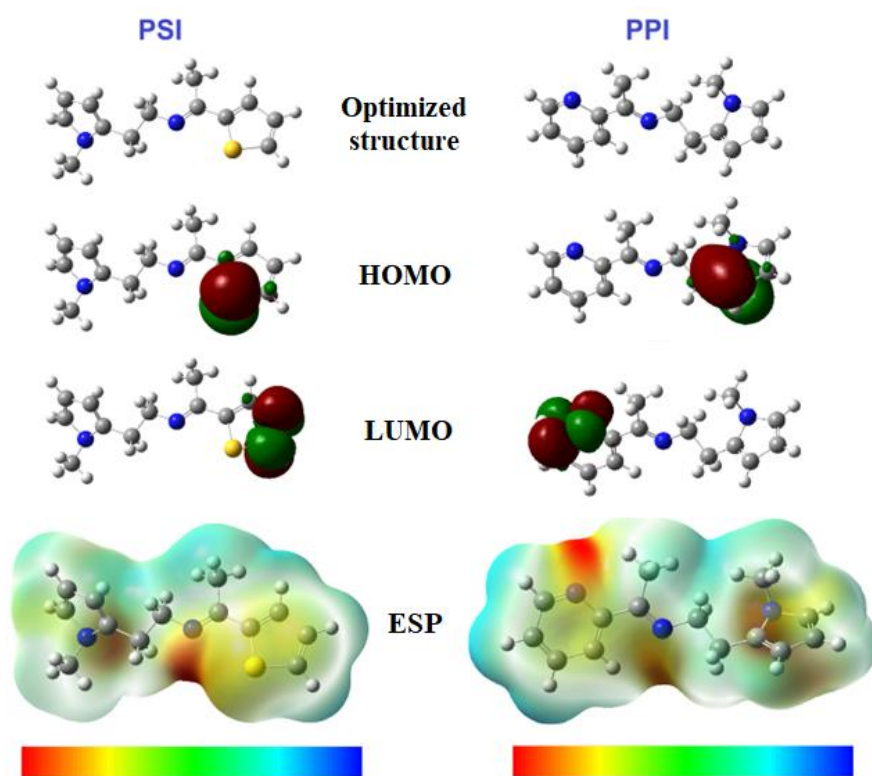


Figure 7. Geometry optimized structures, HOMO, LUMO, and electrostatic potential (ESP) of PSI and PPI inhibitors.

The aptitude to absorb electrons from an electron release chemical as inhibitor particles is often greater on the metal surface with the lowest empty orbital [63]. On the other hand, the metal might, via back connection, discharge its HOMO electrons to the LUMO with a sufficient vacant orbital of the inhibitor particles [64]. The main explanation for the adsorption process of inhibitor particles at metallic substrates is the donor/acceptor interaction between the inhibitor particles and the empty orbitals of metallic surface [65]. The adsorption operations were completed once the HOMO/LUMO interacted via the link between the iron atoms and the CS substrate. The HOMO & LUMO vitalities of PSI and PPI were used to calculate the E_{HOMO} , E_{LUMO} , energy gap ΔE ($E_{\text{LUMO}} - E_{\text{HOMO}}$), electronegativity (χ),

hardness (η), electron affinity (A), ionization potential (I), and electron-transfer-fraction (ΔN), as shown in Table 3.

Table 3. The calculated quantum chemical parameters for PSI and PPI inhibitors

Parameters	PSI	PPI
E_{LUMO}	-0.2597	-0.2384
E_{HOMO}	-0.0196	-0.0574
ΔE	0.2401	0.1810
Ionization (I)	0.2597	0.2384
Affinity (A)	0.0196	0.0574
Absolute electronegativity (χ)	0.1397	0.1479
Global hardness (η)	0.1201	0.0905
ΔN	19.5750	26.1298

Fig. 7 shows how the S-atom of the thiophene ring and the N-atom of the pyrrole ring of the PSI and PPI, respectively, are where the electronic mass of the HOMO component is most widely distributed, demonstrating their capacity for electron release. However, the double bond that is attached to the thiophene ring in PSI and the pyridine ring in PPI, which is responsible for electron uptake, are where the electronic mass of the LUMO component is mostly established. It is widely known that the E_{HOMO} electron-donating capacity and solidity of contact with the metal substrate increase with E_{HOMO} size. Similarly, the rougher the electron-taking acceptance and the firmer the adsorption at the metal substrate are, the smaller the E_{LUMO} is [66,67]. As a result, a smaller value of the energy gap ΔE correlates with a higher adsorption volume, which is advantageous for enhancing the effectiveness of corrosion inhibition. Table 3 shows that PSI's ΔE value is close to PPI's value and indicates that the activity of the two is not considerably different from one another [68]. The seamless planar architecture of PPI and their higher rate of surface covering by adsorption are the main reasons why the inhibitory result of PPI is better than that of PSI. Based on Pearson's idea [69,70], the electron-transfer-fraction (ΔN) of inhibitor particles and the CS substrate was calculated in order to determine the contribution of electrons throughout the corrosion reserve:

$$\Delta N = \frac{(\chi_{Fe} - \chi_{Inh})}{2(\eta_{Fe} + \eta_{Inh})} \quad (6)$$

$$\chi = -\frac{I + A}{2} \quad (7)$$

$$\eta = \frac{I - A}{2} \quad (8)$$

where the variables χ and η stand for, respectively, the electro-negativity and hardness values. The theoretic values of 4.82 and zero were implemented by the factors of χ_{Fe} & η_{Fe} , respectively [71-73]. Ionization potentials and electron affinities are shown by the parameters I ($-E_{HOMO}$) & A ($-E_{LUMO}$), respectively. The analysis shows that the electrons will move from the small electronegativity site to the larger electronegativity location until equilibrium occurs when the metal substrates and the inhibitor particles are close to one another. In general, the electrons flow from the inhibitor particles into the Fe atoms at the CS substrate when the value of electron-transfer-fraction (ΔN) is positive, while the reverse occurs when the value of electron-transfer-fraction (ΔN) is negative, a process known as back-donation

[74]. According to Table 3, PSI and PPI have remarkable abilities to release electrons from the inhibitor's particles to the Fe atom at the CS surface through co-ordination bonds. This results in the production of an effective protective coating and prevents the dissolution of metal [75].

3.5. Molecular dynamic simulation

To fully comprehend the interaction between the studied inhibitor particles and the CS substrate, MD simulations have been run on a Fe(110) substrate [76]. The equilibrium outlines of PSI and PPI inhibitor particles at the CS are depicted in Fig. 8 using the top and side views. At the Fe(110) substrate, both PSI and PPI conformers were consistently and securely absorbed. It makes plausible that the total handling produced by a parallel technique would suspend metallic corrosion when equated to later adsorption instructions [77]. The open *d*-orbitals of the iron atoms on the CS surface are where the electrons from the inhibitor particles travel during the contacting phase, where they create a shield [78].

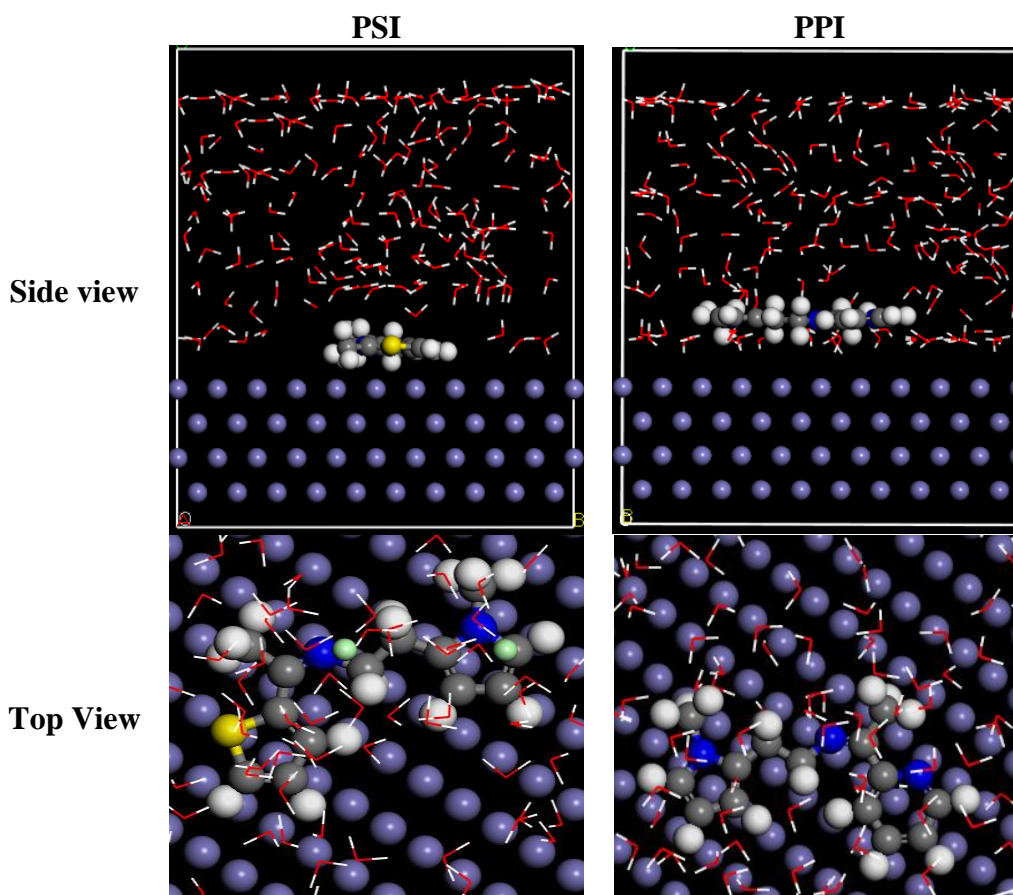


Figure 8. Side and top view for equilibrium adsorption configuration of PSI and PPI inhibitors at the iron surface.

Table 4. Interaction energy and binding energy values between the inhibitors and Fe(110) surface

System	$E_{\text{interaction}}$ (kcal/mol)	E_{binding} (kcal/mol)
Fe + PSI + Formation water	-268.7	268.7
Fe + PPI + Formation water	-295.2	295.2

According to Table 4, the stability of the association between the inhibitor particles and the CS substrate may be inferred from the adsorptive energy. The following equations can be used to specify the interactions between the inhibitor particles being considered at the CS substrate in the reproduction system. These interactions were made possible by the computed interaction-energies ($E_{\text{interaction}}$) and binding-energies (E_{binding}).

$$E_{\text{interaction}} = E_{\text{total}} - (E_{\text{surface+H}_2\text{O}} + E_{\text{inhibitor}}) \quad (9)$$

$$E_{\text{binding}} = -E_{\text{interaction}} \quad (10)$$

The parameter (E_{total}) refers to the combined energy of the CS surface, the considered inhibitor particles, and the H₂O particles. Additionally, the importance of $E_{\text{surface+H}_2\text{O}}$ attitudes to the energy of the corrosive solution and CS surface. The E_{binding} are in the consequent need that the PPI (-295.2 kcal/mol) > PSI (-268.7 kcal/mol) in equilibrium conditions. As a result, PPI particles obtained the highest value of E_{binding} , indicating that they have a more difficult and impulsive adsorptive activity at the CS substrate than PSI particles and, as a result, have a higher percentage inhibitory efficiency of corrosion.

3.6. Mechanism of inhibition

According to experimental and theoretical studies, the suppression of corrosion is efficiently accomplished through a combination of physical and chemical adsorption, via the adsorptive of inhibitor molecules at the CS substrate. The solitary N- and S-atoms of heteroatoms, the aromatic ring's electrons, and the imine (C=N) connection all had significant effects on the chemical adsorption procedure. However, the protonated inhibitor particles in the formation water can physically bind to the negative ions in the CS substrate. However, using the iron atom's electrons at the CS surface would result in more negative ion formation, which would impact how the iron atom's electrons moved during their back-donation to the PSI and PPI particles. The releasing and back-releasing of elections cooperate to enhance PSI and PPI particle adsorptive at the CS substrate. In light of these concepts, it is clear that the investigated PSI and PPI inhibitor s provide potential alternatives for CS corrosion inhibition in the formation water.

3.7. Comparative study

The tested PSI and PPI inhibitors may be regarded as strong corrosion inhibitors for CS formation water based on their protection efficiency statistics when compared to the published data shown in Table 5. The results of the current investigation are in line with those of other studies that used various imine compounds as corrosion inhibitors. The results demonstrated that the Langmuir model is a mixed-type inhibitor and is designated as a common adsorption model.

Table 5. Comparison of the tested compound and other similar inhibitors

Inhibitor	Inhibitor concentration	Corrosive medium	Metal type	Inhibition efficiency (%)	Reference
bis(N,N'-disalicylidene)-1,3-propanediamine-PEG400	600 ppm	Formation water	X65-steel	78.9	[79]
bis(N,N'-disalicylidene)-1,3-propanediamine-PEG600				81.3	
bis(N,N'-disalicylidene)-1,8-octanediamine-PEG400				80.5	
bis(N,N'-disalicylidene)-1,8-octanediamine-PEG600				82.1	
bis(N,N'-disalicylidene)-1,10-decanediamine-PEG400				85.4	
bis(N,N'-disalicylidene)-1,10-decanediamine-PEG600				87.8	
(E)-3-(3-hydroxybenzylideneamino)-2-(3-hydroxyphenyl)-2,3-dihydroquinazolin-4(1H)-one	0.00065 M	2 M HCl	Mild steel	85.5	[80]
(E)-3-(4hydroxybenzylideneamino)-2-(4-hydroxyphenyl)-2,3-dihydroquinazolin-4(1H)-one				77.3	
2,2'-((1Z,1'Z)-(((1,2-phenylenebis(oxy)) bis(2,1-phenylene))bis(methanylylidene))bis(azanylylidene))diethanol	0.002 M	0.5 M H ₂ SO ₄	Carbon steel	76.0	[81]
2,2'-((1Z,1'Z)-((propane-1,3-diylbis(oxy))bis(2,1-phenylene))bis(methanylylidene))bis(azanylylidene))diethanol				79.0	
Bis(N,N'-disalicylidene)-o-pheylenediamine-PEG-400	600 ppm	Formation water	Carbon steel	88.6	[82]
Bis(N,N'-disalicylidene)-o-pheylenediamine-PEG-600				91.1	
Bis(N,N'-disalicylidene)-p-pheylenediamine-PEG-400				93.5	
Bis(N,N'-disalicylidene)-p-pheylenediamine-PEG-600					

4. CONCLUSIONS

A newly created chemical called PSI and PPI is being studied and tested as a corrosion inhibitor in formation water solution. According to potentiodynamic polarization and EIS test methods, PSI and PPI have 83.3% and 89.8%, respectively, and inhibitory efficiency percentages at 1×10^{-3} M. According to Tafel data, these substances have the capacity to postpone anodic and cathodic reactions. According to EIS data, PSI and PPI inhibitors formed an adsorbed layer that increased the CS dissolving resistance in formation water. Through a combination of physical and chemical interactions, the adsorption of both inhibitors followed the Langmuir adsorption isotherm model. DFT calculations indicated the formation of covalent linkages between the active sites of inhibitors and the iron atoms, and their higher affinity for steel surface was supported by their close-knit distribution over hematite surfaces. The investigation's usage of imine compounds revealed them to be possible corrosion inhibitors.

DECLARATION OF COMPETING INTEREST

The authors declare that they have no conflict of interest.

ACKNOWLEDGMENTS

The authors extend their appreciation to the Deanship of Scientific Research at Imam Mohammad Ibn Saud Islamic University, Saudi Arabia for funding this research work through the Research group no. RG-21-09-81.

References

1. L. O. Olasunkanmi, N. I. Aniki, A. S. Adekunle, L. M. Durosinmi, S. S. Durodola, O. O. Wahab, and E. E. Ebenso, *J. Mol. Liq.*, 343 (2021) 117600.
2. N. Karki, S. Neupane, D. K. Gupta, A. K. Das, S. Singh, G. M. Koju, Y. Chaudhary, and A. P. Yadav, *Arab. J. Chem.*, 14 (2021) 103423.
3. M. Heikal, A. Ali, B. S. Ibrahim, A. Toghan, *Constr Build Mater.*, 243 (2020) 118309.
4. A. A. Farag and E. A. Badr, *Corros. Rev.*, 38 (2020) 151.
5. A. A. Khadom, S. A. Jassim, M. M. Kadhim, and N. B. Ali, *J. Mol. Liq.*, 347 (2022) 117984.
6. Y. Konno, A. A. Farag, E. Tsuji, Y. Aoki, and H. Habazaki, *J. Electrochem. Soc.*, 163 (2016) 386.
7. A. G. Al-Gamal, A. A. Farag, E. M. Elnaggar, and K. I. Kabel, *Compos. Interfaces*, 25 (2018) 959.
8. A. Toghan, A. Fawzy, N. Alqarni, A. Abdelkader, A. I. Alakhras, *Int. J. Electrochem. Sci.*, 16 (2021) 211118.
9. H. M. Abd El-Lateef, S. Shaaban, M. M. Khalaf, A. Toghan, K. Shalabi, *Colloids Surf. A: Physicochem. Eng. Asp.*, 625 (2021) 126894.
10. A. A. Farag, E. A. Mohamed, G. H. Sayed, and K. E. Anwer, *J. Mol. Liq.*, 330 (2021) 115705.
11. A. Fawzy, A. Toghan, *ACS Omega*, 6 (2021) 4051-4061.
12. A. Toghan, H. M. Dardeer, H. S. Gadow, H. M. Elabbasy, *J. Mol. Liq.*, 325 (2021) 115136.
13. A. A. Farag, *Corros. Rev.*, 36 (2018) 575.
14. A. Toghan, M. Gouda, K. Shalabi, H. M. Abd El-Lateef, *Polymers*, 13 (2021) 2275.
15. K. I. Kabel, A. A. Farag, E. M. Elnaggar, and A. G. Al-Gamal, *J. Superhard Mater.*, 37 (2015) 327.
16. K. I. Kabel, A. A. Farag, E. M. Elnaggar, and A. G. Al-Gamal, *Arab. J. Sci. Eng.*, 41 (2016) 2211.
17. B. Arifa Farzana, A. Mushira Banu, and K. Riaz Ahamed, *Mater. Today Proc.*, 47 (2021) 2080.
18. A. Farag, E. Mohamed, A. Toghan, *Corros. Rev.*, (2022), in press.
19. A. A. Farag, A. Toghan, M. S. Mostafa, C. Lan, G. Ge, *Catalysts*, 12 (2022) 838.
20. M. A. Migahed, A. A. Farag, S. M. Elsaed, R. Kamal, and H. Abd El-Bary, in *Eur. Corros. Congr. 2009, EUROCORR 2009* (2009).
21. P. Rugmini Ammal, M. Prajila, and A. Joseph, *Egypt. J. Pet.*, 27 (2018) 307.
22. X.-L. Li, B. Xie, J.-S. Feng, C. Lai, X.-X. Bai, T. Li, D.-L. Zhang, W.-Y. Mou, L. Wen, and Y.-T. Gu, *J. Mol. Liq.*, 345 (2022) 117032.
23. A. E. L. Aatiaoui, M. Koudad, T. Chelfi, S. Erkan, M. Azzouzi, A. Aouniti, K. Savaş, M. Kaddouri, N. Benchat, and A. Oussaid, *J. Mol. Struct.*, 1226 (2021) 129372.
24. S. Sengupta, M. Murmu, N. C. Murmu, and P. Banerjee, *J. Mol. Liq.*, 326 (2021) 115215.
25. S. K. Saha, M. Murmu, N. C. Murmu, and P. Banerjee, *J. Mol. Struct.*, 1245 (2021) 131098.
26. M. El Azzouzi, K. Azzaoui, I. Warad, B. Hammouti, S. Shityakov, R. Sabbahi, S. Saoiabi, M. H. Youssoufi, N. Akartasse, S. Jodeh, A. Lamhamdi, and A. Zarrouk, *J. Mol. Liq.*, 347 (2022) 118354.
27. A. Berrissoul, A. Ouarhach, F. Benhiba, A. Romane, A. Guenbour, H. Outada, A. Dafali, and A. Zarrouk, *J. Mol. Liq.*, 349 (2022) 118102.
28. K. Zhang, B. Xu, W. Yang, X. Yin, Y. Liu, and Y. Chen, *Corros. Sci.*, 90 (2015) 284.
29. M. E. Mashuga, L. O. Olasunkanmi, H. Lgaz, E.-S. M. Sherif, and E. E. Ebenso, *J. Mol. Liq.*, 344 (2021) 117882.
30. W. Zhang, B. Nie, H.-J. Li, Q. Li, C. Li, and Y.-C. Wu, *Carbohydr. Polym.*, 260 (2021) 117842.
31. D. Zhang, L. Li, L. Cao, N. Yang, and C. Huang, *Corros. Sci.*, 43 (2001) 1627.
32. E. S. Ferreira, C. Giacomelli, F. C. Giacomelli, and A. Spinelli, *Mater. Chem. Phys.*, 83 (2004) 129.
33. S. M. Shaban, E. a Badr, M. A. Shenashen, and A. A. Farag, *Environ. Technol. Innov.*, 23 (2021) 101603.
34. S. About, D. Chebabe, M. Zouarhi, M. Rehioui, Z. Lakbaibi, and N. Hajjaji, *J. Mol. Struct.*, 1240 (2021) 130611.
35. H. M. Abd El-lateef, H. S. El-Beltagi, M. E. Mohamed, M. Kandeel, E. Bakir, A. Toghan, K. Shalabi, M. M. Khalaf, *Front. Materials*, 9 (2022) 843438.

36. A. G. Al-Gamal, T. H. Chowdhury, K. I. Kabel, A. A. Farag, N. E. A. Abd El-Sattar, A. M. Rabie, and A. Islam, *Sol. Energy*, 228 (2021) 670.
37. B. Kumar, H. Vashisht, M. Goyal, A. Kumar, F. Benhiba, A. K. Prasad, S. Kumar, I. Bahadur, and A. Zarrouk, *J. Mol. Liq.*, 318 (2020) 113890.
38. C. Wang, C. Zou, and Y. Cao, *J. Mol. Struct.*, 1228 (2021) 129737.
39. F. Bentiss, M. Lebrini, and M. Lagrenée, *Corros. Sci.*, 47 (2005) 2915.
40. E. Bayol, T. Gürten, A. A. Gürten, and M. Erbil, *Mater. Chem. Phys.*, 112 (2008) 624.
41. Y. Qiang, S. Zhang, B. Tan, and S. Chen, *Corros. Sci.*, 133 (2018) 6.
42. A. A. Farag, H. E. Abdallah, E. A. Badr, E. A. Mohamed, A. I. Ali, and A. Y. El-Etre, *J. Mol. Liq.*, 341 (2021) 117348.
43. E. A. Mohamed, H. E. Hashem, E. M. Azmy, N. A. Negm, and A. A. Farag, *Environ. Technol. Innov.*, 24 (2021) 101966.
44. H. Hamani, T. Douadi, D. Daoud, M. Al-Noaimi, R. A. Rikkouh, and S. Chafaa, *J. Electroanal. Chem.*, 801 (2017) 425.
45. R. Solmaz, G. Kardaş, M. Çulha, B. Yazıcı, and M. Erbil, *Electrochim. Acta*, 53 (2008) 5941.
46. H. Ashassi-Sorkhabi, B. Shaabani, and D. Seifzadeh, *Appl. Surf. Sci.*, 239 (2005) 154.
47. M. Lagrenée, B. Mernari, M. Bouanis, M. Traisnel, and F. Bentiss, *Corros. Sci.*, 44 (2002) 573.
48. A. Amer, G. H. Sayed, R. M. Ramadan, A. M. Rabie, N. A. Negm, A. A. Farag, and E. A. Mohammed, *J. Mol. Liq.*, 341 (2021) 116935.
49. A. A. Altalhi, E. A. Mohammed, S. S. M. Morsy, N. A. Negm, and A. A. Farag, *Fuel*, 295 (2021) 120646.
50. H. A. Abubshait, A. A. Farag, M. A. El-Raouf, N. A. Negm, and E. A. Mohamed, *J. Mol. Liq.*, 327 (2021) 114790.
51. S. Martinez and I. Stern, *Appl. Surf. Sci.*, 199 (2002) 83.
52. A. Dutta, S. K. Saha, U. Adhikari, P. Banerjee, and D. Sukul, *Corros. Sci.*, 123 (2017) 256.
53. M. Galai, M. Rbaa, M. Ouakki, A. S. Abousalem, E. Ech-chihbi, K. Dahmani, N. Dkhireche, B. Lakhrissi, and M. EbnTouhami, *Surf. Interfaces.*, 21 (2020) 100695.
54. D.-Y. Wang, B.-L. Nie, H.-J. Li, W.-W. Zhang, and Y.-C. Wu, *J. Mol. Liq.* 331, 115799 (2021).
55. K. F. Khaled, *Electrochim. Acta*, 53 (2008) 3484.
56. P. Singh, V. Srivastava, and M. A. Quraishi, *J. Mol. Liq.*, 216 (2016) 164.
57. A. Zarrouk, B. Hammouti, T. Lakhlifi, M. Traisnel, H. Vezin, and F. Bentiss, *Corros. Sci.*, 90 (2015) 572.
58. Y. Tang, F. Zhang, S. Hu, Z. Cao, Z. Wu, and W. Jing, *Corros. Sci.*, 74 (2013) 271.
59. V. V. Torres, V. A. Rayol, M. Magalhães, G. M. Viana, L. C. S. Aguiar, S. P. Machado, H. Orofino, and E. D'Elia, *Corros. Sci.*, 79 (2014) 108.
60. R. Solmaz, *Corros. Sci.*, 52 (2010) 3321.
61. J. Saranya, F. Benhiba, N. Anusuya, R. Subbiah, A. Zarrouk, and S. Chitra, *Colloids Surfaces A Physicochem. Eng. Asp.*, 603 (2020) 125231.
62. H. E. Hashem, E. A. Mohamed, A. A. Farag, N. A. Negm, and E. A. M. Azmy, *Appl. Organomet. Chem.*, 35 (2021) 6322.
63. M. Murmu, S. K. Saha, N. C. Murmu, and P. Banerjee, *Corros. Sci.*, 146 (2019) 134.
64. A. A. Farag, M. A. Migahed, and E. A. Badr, *J. Bio-Tribo-Corrosion*, 5 (2019) 53.
65. A. Saxena, D. Prasad, and R. Haldhar, *Bioelectrochemistry*, 124 (2018) 156.
66. H. Lgaz, K. Subrahmanya Bhat, R. Salghi, Shubhalaxmi, S. Jodeh, M. Algarra, B. Hammouti, I. H. Ali, and A. Essamri, *J. Mol. Liq.*, 238 (2017) 71.
67. W. Li, Q. He, C. Pei, and B. Hou, *Electrochim. Acta*, 52 (2007) 6386.
68. D. K. Singh, E. E. Ebenso, M. K. Singh, D. Behera, G. Udayabhanu, and R. P. John, *J. Mol. Liq.*, 250 (2018) 88.
69. N. Bhardwaj, P. Sharma, L. Guo, O. Dagdag, and V. Kumar, *J. Mol. Liq.*, 346 (2022) 118237.
70. M. J. Momeni, H. Behzadi, P. Roonasi, S. A. S. Sadjadi, S. M. Mousavi-Khoshdeld, and S. V.

- Mousavi, *Res. Chem. Intermed.*, 41 (2015) 6789.
71. V. Srivastava, J. Haque, C. Verma, P. Singh, H. Lgaz, R. Salghi, and M. A. Quraishi, *J. Mol. Liq.*, 244 (2017) 340.
72. M. Yadav, D. Behera, S. Kumar, and P. Yadav, *Chem. Eng. Commun.*, 202 (2015) 303.
73. C.-G. Zhan, J. A. Nichols, and D. A. Dixon, *J. Phys. Chem. A*, 107 (2003) 4184.
74. H. E. Hashem, A. A. Farag, E. A. Mohamed, and E. M. Azmy, *J. Mol. Struct.*, 1249 (2022) 131641.
75. A. Singh, K. R. Ansari, P. Banerjee, M. Murmu, M. A. Quraishi, and Y. Lin, *Colloids Surfaces A Physicochem. Eng. Asp.*, 623 (2021) 126708.
76. A. A. Farag, A. M. Eid, M. M. Shaban, E. A. Mohamed, and G. Raju, *J. Mol. Liq.*, 336 (2021) 116315.
77. K. E. Anwer, A. A. Farag, E. A. Mohamed, E. M. Azmy, and G. H. Sayed, *J. Ind. Eng. Chem.*, 97 (2021) 523.
78. A. A. Farag, A. S. Ismail, and M. A. Migahed, *J. Bio- Tribo-Corrosion*, 6 (2020) 16.
79. M.A. Migahed, A.A. Farag, S.M. Elsaed, R. Kamal, M. Mostfa, H. Abd El-Bary, *Mater. Chem. Phys.*, 125 (2011) 125–135.
80. Arjun G. Kalkhambkar, S.K. Rajappa, *Adv. Chem. Eng.*, 12 (2022) 100407.
81. H. Jafari, E. Ameri, M. Rezaeivala, A. Berisha, J. Halili, *J Phys Chem Solids*, 164 (2022) 110645.
82. M.A. Migahed, A.A. Farag, S.M. Elsaed, R. Kamal, H. Abd El-Bary, *Chem. Eng. Comm.*, 199 (2012) 1335–1356.